DECREASED RESILIENCE OF MANGROVES STRESSED BY HUMAN INTERFERENCE.

P.W.J.M. Willemsen, E. M. Horstman, B. W. Borsje, D. A. Friess, C.M. Dohmen-Janssen

ABSTRACT

Biophysical feedback mechanisms are essential to maintain mangroves. These mechanisms facilitate sediment deposition during periods of tidal flooding and stabilize mangroves. However, human interference (e.g. sediment starvation and coastal squeeze) affects these biophysical interactions. This paper shows the impacts of human interference, i.e. sediment starvation and coastal squeeze, on the biophysical interactions in mangroves.

Field data of hydrodynamics and sediment dynamics were obtained in a fringing estuarine mangrove in the Straits of Johor, located at the northern shores of Singapore. An accurate depth-averaged process-based numerical model was developed in Delft3D, showing reasonable approximations of flow velocities and deposition rates. Simulations with this model provided insight in the instantaneous response of the mangrove when sediment starvation and coastal squeeze were reduced.

The model results show increased deposition rates within the mangrove when sediment supplies were restored. A reduction of the coastal squeeze by extending the intertidal area in the inland directions results in increasing flow velocities and deposition rates as well. A comparison between these scenario runs and the current state of the mangrove shows a decrease in biophysical interaction and even a total loss of the contribution of vegetation to the stability of the current state mangrove. The human interference, contributing to sediment starvation and coastal squeeze, has evidently decreased the mangrove's resilience. More importantly, relieving these human induced stresses, found to enhance sediment deposition rates, facilitates an increased resilience to future changes such as sea-level rise.

KEYWORDS

Mangroves; biophysical interactions; numerical model; mangrove degradation; sediment starvation; coastal squeeze.

1. INTRODUCTION

Worldwide, mangroves provide indispensable services to nature and mankind and yet they are highly threatened by human interference. Conversion of these intertidal wetlands for purposes such as industrialization, aquaculture, agriculture and subsistence uses are causing a rapid decrease of the mangrove area (e.g. Valiela et al. 2001; Kirwan et al. 2013; Webb et al. 2014). With an average area loss of 2.1% per year since the early 1980s, mangrove losses exceed those of tropical rain forests and coral reefs (Valiela et al. 2001; Duarte et al. 2008). Mangroves are also threatened by long-term and indirect anthropogenic influences, such as sea-level rise (SLR), decreased sediment supply rates and reduced possibilities of landward migration space (Thampanya et al. 2006; Kirwan et al. 2013; Krauss et al. 2014). Mangroves can adapt to such direct and indirect anthropogenic stresses, and combinations thereof, as long as certain physical and ecological thresholds are not exceeded (Friess et al. 2012). The resilience of mangroves acts within these species-specific habitat constraints and is facilitated by a complex system of biophysical interactions, consisting of ecosystem engineering mechanisms operating at a range of different scales (Friess et al. 2012).

Biophysical feedback mechanisms in mangroves imply that the accretion tends to follow sea-level rise (Webb et al. 2013; Krauss et al. 2014). As sediment deposition is facilitated during periods of tidal flooding, sediment deposition could increase in vegetated intertidal areas with a lower elevation with respect to mean sea level (MSL). Adequate vegetation densities attenuate tidal flows and wind waves in these areas, enhancing local sediment deposition rates (Friess et al. 2012; Horstman et al. 2015). Increased deposition allows for the vegetation to expand, further enhancing the sediment trapping potential of the mangrove. Fine root mats with high root densities are most effective in slowing down hydrodynamics and accreting sediments (Krauss et al. 2003). Meanwhile, expanding vegetation also adds to the surface elevation by means of the increase of

organic matter (roots) in the subsurface (Kirwan et al. 2013). This positive feedback loop is a typical feature of ecosystem engineers–organisms that change their abiotic environment to their own benefit (Jones et al. 1994; Jones et al. 1997).

The biophysical resilience of mangroves depends to a great extent on sediment concentrations in the surrounding region (Kirwan et al. 2010; Kirwan et al. 2013). Surface elevation in mangroves could adapt to SLR, provided that suspended sediment inputs are sufficient (e.g. Victor et al. 2004; Thampanya et al. 2006). In response to SLR, mangroves face increased tidal inundation (times and depths) and hence an increasing sediment influx, setting off the biophysical feedbacks (Mckee et al. 2007; Krauss et al. 2010). However, anthropogenic influences are severely affecting sediment supply to the coastal zone, resulting in sediment starvation of the mangroves. Globally, reservoirs trap no less than 26% of the total terrestrial sediment discharge, reducing the influx of sediments to the coastal system (Syvitski et al. 2005). Hence, ongoing river damming has the potential to severely reduce the accretion capacity of mangroves (Horstman et al. 2015).

Coastal squeeze is another widespread human induced impact that stresses mangroves (Doody 2004). SLR requires mangroves to trap sufficient sediments and/or to extend inland as to induce an elevation gain that offsets the rate of SLR, so the entire mangrove system maintains its relative position in the tidal frame (Friess et al. 2012). In case the inundation frequency and period of a mangrove increase and its landward adaptation space is limited, the mangrove is squeezed between the rising sea level and the anthropogenic environment. Subsequently, mangrove vegetation cannot survive when biophysical thresholds of the positive ecosystem engineering feedbacks are exceeded, giving rise to 'ecological drowning' (Friess et al. 2012). The latter can occur in case the rate of SLR exceeds the elevation gain within the mangroves, eventually causing the physical parameters of inundation frequency and period to exceed a threshold of species-specific inundation tolerance.

Horstman et al. (2015) indicate that undisturbed mangroves are highly sensitive to climate change and anthropogenic stresses. However, knowledge on the consequences of reduced sediment supply on the perseverance of mangrove forests is limited (Thampanya et al. 2006). Consequently, this raises questions about the resilience of stressed mangroves that have already been affected by human interference and where negatively influenced feedback mechanisms are the status quo. Knowledge about the resilience and development of anthropogenic affected mangroves, stressed by e.g. sediment starvation and coastal squeeze, is lacking as well. This knowledge gap has been identified by Kirwan et al. (2013), addressing the incorporation of the indirect effects of human interference on e.g. sediment availability as a key challenge for future modeling attempts of coastal wetland evolution . Such models will help addressing the consequences of sediment starvation and coastal squeeze on mangroves and are key to a better understanding of the perseverance of both affected and unaffected mangroves, one of our most valuable and yet most threatened ecosystems (Valiela et al. 2001; De Groot et al. 2012).

The aim of this paper is to gain insight in the biophysical interactions in disturbed mangroves stressed by sediment starvation and coastal squeeze. This is achieved by (I) obtaining field observations of the hydrodynamics and sediment dynamics of an estuarine mangrove forest in Singapore that has long been stressed by human interference, and (II) identifying the potential resilience of stressed mangroves under reduced sediment starvation and coastal squeeze by means of a numerical scenario analysis. Field observations were used to calibrate and validate a numerical, process-based model (Delft3D) that was set-up to simulate hydrodynamics and sediment dynamics in the study area. The calibrated model provides an ideal platform to analyze the impact of coastal squeeze and sediment starvation by simulating the instantaneous response of the disturbed mangroves to these conditions.

This paper starts with an introduction to the data collection methods deployed in the field and the subsequent model set-up and calibration with these data (section 2). Results of the sensitivity analysis, proving the accuracy of the model, and the scenario analysis, identifying differences in the resilience of the mangrove when facing reduced stresses, are presented in section 3. The main findings of this paper are discussed in section 4, leading to general conclusions summarized in section 5.

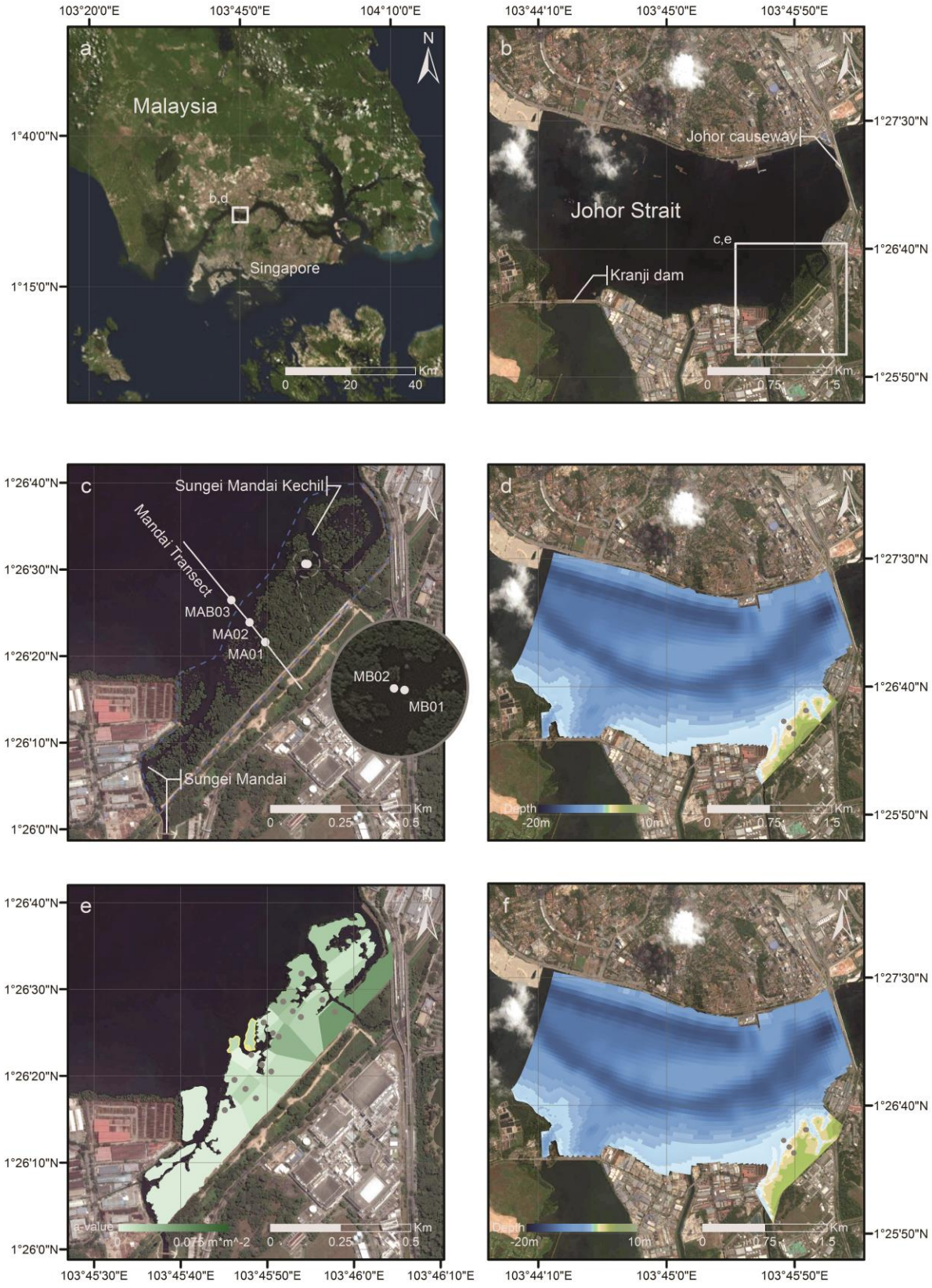

Figure 1. (a) Singapore and Southern Malaysia surrounded by the Malacca Strait, Singapore Strait and the South China Sea. (b) The Straits of Johor with the Mandai mangrove. (c) Mandai mangrove including measurement locations and mangrove extent (blue dashed outline). (d) Bathymetry used in the Delft3D model (Kernkamp et al. 2005) overlying The Straits of Johor and Mandai mangrove. (e) Vegetation polygons in the model showing averaged vegetation data, based on the measurement plots (Lee 2015) showed by the gray

dots. The vegetation density, quantified as average tree diameter [m] times average stem density [m^{-2}], is shown by the green gradient (obtained through nearest-neighbor interpolation between measurement plots). The yellow outlined polygons show the Sonneratia patches measured during this study. (f) Extended model at the back of Mandai for the scenario analysis. (Service layer credits panel a: Esri, DigitalGlobe, GeoEye, i-cubed, USDA, USGS, AEX, Getmapping, Aerogrid, IGN, IGP, swisstopo, and the GIS User Community. Service layer credits panel b-f: Google Earth)

2. METHODS

2.1. STUDY SITE

Mandai mangrove (1°26'21''N; 103°45'49''E), which is located at the northern shores of Singapore, covers approximately 15.4 ha of intertidal area (Yee et al. 2010) and was once part of an extensive mangrove forest along the Singapore coast. Inland, Mandai mangrove is enclosed by the former Singapore-Malaysia railway and the rivers Sungei Mandai (Besar) and Sungei Mandai Kechil discharging into the area, at the southwestern and northeastern side respectively (Fig. 1.b). To the northeast part, the Johor causeway closes off the Straits of Johor and at the southwestern side the Sungei Kranji is dammed too.

Figure 2. (a) Fragmented and scattered pattern of vegetation at Mandai's mangrove fringe, including some old and dead trees. (b) Sonneratia sapling establishment in front of the mangrove.

Mandai can be classified as a fringing mangrove forest (Mazda et al. 2007), which is situated in an estuary and is exposed to semi-diurnal tides with a mean tidal range of approximately 2.6 m (3.9 m at spring tides). Wave exposure is very limited due to the limited fetch in front of the mangrove. The vegetation primarily consists of the low elevation pioneer species *Avicennia alba* and *Sonneratia alba* at the seaward fringe. Further landward, the diverse back mangrove includes *Bruguiera cylindrica*, *B. gymnorrhiza, Excoecaria agallocha* and *Lumnitzera racemosa* (Friess et al. 2012). The vegetation shows a fragmented and scattered pattern with an erosive trend with old trees at the mangrove fringe (Fig. 2.a) and newly establishing seedlings and saplings in front of the mangrove (Fig 2.b).

Field data have been collected in March and April 2015, at five different locations throughout the forest (Fig. 1.c), giving a thorough representative view of the mangrove: location MA01 is situated in the elevated back of the mangrove forest vegetation; MA02 is located at the mangrove fringe within an extensive patch of recently established *Sonneratia* saplings; MAB03 is located at the mudflat; MB01 is positioned in a tidal creek discharging in the Sungei Mandai Kechil outlet and MB02 is located at the adjacent creek bank.

2.2. FIELD DATA COLLECTION

2.2.1. Vegetation characteristics

An extensive vegetation study was conducted in February and March 2015 by Lee (2015), wherein vegetation characteristics were measured in 17 plots with a diameter of 7 m per plot (Fig 1.e; gray dots), over a total of five cross-shore transects. Mangrove trees exceeding 5 cm diameter at breast height (DBH equal to 1.30 m), within the plots, were measured. The species as well as the diameter at DBH were collected. In addition saplings, representing all trees with a diameter below 5 cm at DBH, were counted for all plots (Lee 2015). It was assumed that the saplings in general had a diameter of 2.5 cm. This study did not include the recently appeared *Sonneratia* patches in front of the established vegetation and at the mudflat, due to the height of the major part of this vegetation (not exceeding DBH). The outlines of these patches of *Sonneratia* saplings, as well as one patch of *Sonneratia* trees were mapped during the present study, in March/April 2015, using a Garmin GPSMAP 62s. *Sonneratia* saplings (Fig. 2.b) were sampled within a random chosen representative plot with a radius of 7.0 m. The stem diameter was measured at the bottom and at breast height. *Sonneratia* trees (five) were sampled by measuring the diameter at the bottom and at breast height. Due to the maximum water levels during high tide at this site, the canopy of the trees is not flooded and hence will not impact the hydrodynamics and sediment dynamics under regular conditions. Tree characteristics were averaged to obtain a single characteristic tree or sapling per plot. The representative plot with saplings was extrapolated to the two mapped patches and the measured trees were extrapolated to the measured patch with *Sonneratia* trees.

2.2.2. Hydrodynamics

Hydrodynamics were mapped by monitoring flow velocities in horizontal (x, y) and vertical (z) directions, with Nortek Acoustic Doppler Velocimeters (ADVs). The ADV heads were mounted downward looking, measuring flow velocities at 0.07 m above the bed. A minimum water depth of approximately 0.25 m was required for data collection by the ADVs. To reduce flow disturbance, the mounting of the ADVs was oriented perpendicular to the prevailing flow directions of the tides. Probe heads were mounted and aligned to the north. The set-up of the ADVs was similar to the set-up used by Horstman et al. (2013), resulting in minor disturbances. The sampling rate of the ADV's was 16 Hz, with 600 seconds per burst and a burst interval of 10 minutes.

Data was collected during multiple tidal cycles, with the instruments being deployed and retrieved at two subsequent low tides: hydrodynamics at the back of the forest (MA01), the mangrove fringe (MA02) and the mudflat (MAB03, see Fig. 1c) were monitored during two individual near-spring high tides (24 March 2015 and 5 April 2015); and data were collected at the tidal creek (MB01), the tidal creek bank (MB02) and the mudflat (MAB03) during two different near-spring high tides (25 March 2015 and 6 April 2015). Flow velocities at location MAB03 were measured during all deployments for reference.

The obtained hydrodynamic data was pre-processed using filtering, averaging and data correction procedures from Horstman et al. (2013). Inaccurate data was filtered by removing data with a mean correlation of the return signal below 80% (SonTek 1997; Chanson et al. 2008). With the filtering procedure all irrelevant disturbances (e.g. due to shipping, animal activity or air bubbles) were removed. After filtering, the data was averaged over the 10 min bursts to remove fluctuations caused by wind and swell waves. The filtering provided continuous data series during the monitored high tides.

2.2.3. Sediment deposition rates

Sediment deposition rates at Mandai were measured using sediment traps. Our traps were 0.20 m x 0.20 m acrylic sheets, roughened with sandpaper to mimic the natural bottom roughness in the mangrove, similar to the traps in Horstman et al. (2015). These traps were installed flush with the surrounding bed and secured with metal pins. Data was collected using three sediment traps at the back forest (MA01), the mangrove fringe (MA02), the tidal creek (MB01) and the tidal creek bank (MB02) during the respective deployments at these sites, whereas one sediment trap was deployed at the mudflat (MAB03) during all four

periods. The sediment traps were rinsed with de-ionized water to collect the deposits. The dissolved deposits were filtered with pre-weighted filters (0.7µm Whatman GF/F filters), which were dried in the oven (105^{o}C; 24 hours) and weighted again.

In addition, sediment characteristics were analysed for samples from the mobile top layer (<20 mm) at all measurement locations. Two undisturbed samples were retrieved from each location. Each sample was oven-dried (105^{o}C; 24 hours) and lyophilised prior to a grain size analysis and an organic matter content analysis. Grain size analysis of the dry sieved samples (2 mm mesh size) was performed with a particle size analyser (Malvern Mastersizer 2000). The organic matter content was determined by the weight loss upon ashing the dry sieved samples (550^{o}C; 4 hours).

2.3. MODEL SET-UP

2.3.1. Model description

Similar to previous modeling efforts in mangroves (and salt marshes), this study applies the Delft3D software developed by Deltares (e.g. Temmerman et al. 2005). The Delft3D-FLOW module solves the unsteady shallow-water equations in two (depth-averaged) or three dimensions. The system of equations consists of the horizontal momentum equations, the continuity equation, the sediment transport equation, and a turbulence closure (Lesser et al. 2004). Depth-averaged settings were used for this study, since extensive test runs showed that the results of the depth-averaged model were similar to those of the 3D model (see also Hu et al. 2009; Horstman et al. 2015). In addition, this depth-averaged model run can be executed within 8% of the time of a 3D model run (10 layers). The FLOW-module explicitly incorporates the influence of rigid cylindrical plant structures on drag and turbulence in its 3D vegetation model (Deltares 2015).

2.3.2. Model domain

The model domain consists of Mandai mangrove and the nearby section of the Straits of Johor (Fig. 1d). The modal domain has a length of approximately 4.0 km and a width of approximately 2.5 km. The grid and topography were cropped from the hydrodynamic Singapore Regional Model (SRM), that has been developed to provide accurate tidal information in the Singapore Strait region and that is previously described as the Malacca Straits model in Kernkamp et al. (2005). The SRM has been extensively validated (e.g. Kurniawan et al. 2011) and has been further refined and aligned with the depth contours by Hasan et al. (2012).

2.3.3. Topography, vegetation cover and bed roughness

The model extent is enclosed by the former Singapore-Malaysia railway and the Kranji Dam at the southern side, by the Johor Causeway at the eastern side and by the Malaysian embankment at the northern side. The grid has been cut off west of Mandai. The model extent is subdivided using a spherical curvilinear grid, taking the curvature of the earth into account. The grid cells are typically 10 m x 10 m within the study area (Mandai mangrove) and gradually increase in size up to 50 m x 50 m in the Straits of Johor. The maximum elevation is equal to 4.00 m above MSL in the back of the mangrove and the maximum depth is equal to -16.67 m below MSL in the central parts of the Straits of Johor.

The vegetation included in the vegetation model was collected during an extensive study by Lee (2015) and was expanded with extra data collected during this study (see section 2.2.1.). The outline of the vegetation was determined using recent Google Imagery from 6 March 2015, within the period of the vegetation measurements. Grid cells within the outline of the mangrove vegetation received the vegetation characteristics from the nearest measurement plot, resulting in different vegetation zones. Vegetation characteristics were standardized to densities per unit area and an average stem diameter per zone for representation in the vegetation model (Fig. 1.e). Vegetation data observed in the field, beyond the vegetation outlines was added to the model using three extra zones (Fig. 1.e; yellow outlined patches) for which the obtained vegetation characteristics were averaged (Table 1) and added to the vegetation model.

The applied bed roughness value has been obtained from the SRM: a Manning bed roughness coefficient of 0.03 s $m^{-1/3}$ was specified throughout the model domain (in x- and y-direction).

2.3.4. Hydrodynamic boundary condition

The model contains one open boundary in the Straits of Johor, at the western side of the model extent. The Sungei Mandai (Besar) and the Sungei Mandai Kechil (Fig. 1c) were both modeled as closed boundaries due to their very limited (under regular conditions), controlled discharge. The water levels at the remaining open boundary of the model have been analyzed using a two-months model run of a model nested in the SRM. The water levels from the SRM at the location of the open boundary (midpoint of open boundary) of the model were analyzed with the T-Tide Harmonic Analysis Toolbox (Pawlowicz et al. 2002), resulting in 33 tidal constituents, with the dominant constituents being the semidiurnal M2 and S2 constituents and the diurnal O1 and K1 constituents, similar to the findings by Hasan et al. (2012). The full tidal spectrum was imposed as a boundary condition to the present model. Water levels computed with the SRM and the present model (with the imposed tidal boundary condition) were nearly equal (R^2=0.99) near the mangroves.

2.3.5. Sediment dynamics

Sediment dynamics were not included in the SRM and have been added to the model by assuming a uniform cohesive, fine sediment with a constant settling velocity. The sandy fractions (Fig. 4) were neglected as the flow velocities in the study area are too small to transport (substantial amounts of) sands in suspension. Default values were used for the reference density and specific density: 1600 and 2650 kg m^{-3}, respectively (Deltares 2015). The dry bed density was set to 1200 kg m^{-3}, which is within the range of values in Van Santen et al. (2007), and represents densities that are common for estuarine mud (Whitehouse et al. 2000).

The model starts out with a fixed bed, which cannot be brought into suspension. An initial sediment layer at the bed was neglected, because the sediments in this layer show different behavior than the suspended sediments. Nevertheless, deposited sediments were able to be re-entrained.

The boundary condition for suspended sediment concentrations (SSCs) at the open boundary was specified using the data presented in Van Maren et al. (2014), for the east side of the Straits of Johor. The SSCs at the east side of the Johor Causeway, at different relative levels above the bed, were in the range of 10 – 20 mg l^{-1}. Therefore, the suspended sediment concentration at the open boundary was set at 15 mg l^{-1} in the model.

The settling velocity of the modeled sediment fraction was based on the data collected in the field (Table 2). At tidal flats, next to the particle size, the settling velocity is also affected by flocculation, hindered settling, lag effects, etc. (Winterwerp 2002; Van Maren et al. 2012). Hence, it is impossible to exactly define a settling velocity based on the grain size distribution of the fine sediments alone (clay and silt, Fig. 4). Flocculation of the fine-grained sediments, causing the settling velocity to increase, depends on the turbulent energy and sediment concentrations and hence results in spatially and temporarily varying settling velocities (Van Maren et al. 2012). Settling velocities of cohesive sediment in shallow tidal waters generally range between 0.1 and 1 mm s^{-1} (Wolanski et al. 1992; Van Maren et al. 2012). In this study a settling velocity of 0.1 mm s^{-1} was adopted, this is at the lower end of the above mentioned range, and this settling velocity was extensively varied for sensitivity analysis.

Values for the erosion parameter, critical bed shear stress for erosion and critical bed shear stress for sedimentation were assumed to be uniform over the entire model extent. Default values were used for the critical bed shear stresses for erosion and sedimentation, i.e. $5 \cdot 10^{-1}$ N m^{-2} and $1 \cdot 10^{3}$ N m^{-2}, respectively (table 3). A default value was used as well for the erosion parameter, i.e. $1 \cdot 10^{-4}$ kg m^{-2} s^{-1} (table 3) (Deltares 2015).

3. RESULTS

3.1. FIELD OBSERVATIONS

3.1.1. Vegetation

The vegetation characteristics of the *Sonneratia* patches were normalized to densities per square meter (Table 1), based on the data collected in the representative plots for the *Sonneratia* saplings and *Sonneratia* trees. The stem density of the patches with saplings (0.3638 m^{-2}) were more than two times larger than the stem density of the patch with *Sonneratia* trees (0.1516 m^{-2}). The more mature *Sonneratia* trees show diameters (0.061 m) almost two times greater than the *Sonneratia* saplings (0.36 m). The saplings were branching close to the bed (Table 1). The *Sonneratia* saplings were almost entirely covered with barnacles, significantly adding to the dimensions and weight of their stems and branches. The trees were similarly covered with barnacles, generally below the level of inundation.

Vegetation densities measured by Lee (2015) , ranged from 0.019 to 0.331 m^{-2}, with stem diameters ranging from 0.058 to 0.212 m (Fig. 1.e). The amount of saplings counted in the different plots ranged from 4 to 74 (Lee 2015).

Table 1. Characteristics of the patches with Sonneratia saplings, based on the measurements within the plots with Sonneratia saplings and characteristics of the patch with Sonneratia trees.

ID [-]	patch	DBH $[m]$	Diameter bed [m]	Height [m]	Height of branching [m]	Diameter of branches [m]	Number of branches $[-]$	Surface [m^2]	Stem density [m^{-2}]
SS1	**Saplings**	-	0.036	1.120	0.121	0.029	1.66	3073	0.3638
SS2	**Saplings**	-	0.036	1.120	0.121	0.029	1.66	1621	0.3638
ST1	**Trees**	0.039	0.061	>2.0	>2.0	-	-	560	0.1516

3.1.2. Hydrodynamics

Flow velocities measured in Mandai mangrove were generally lower than 10 cm s^{-1} (Fig. 3) and are low compared to velocities observed in other studies (e.g. Van Santen et al. 2007; Horstman et al. 2013). The tidal in- and outflows clearly show an asymmetrical pattern: a small velocity peak was observed during early flood tides and an extended peak of sluggish flow was identified during subsequent ebb tides. The data also showed a distinct decrease in the flow velocities from the front of the mangrove (mudflat) to the higher elevated and denser vegetated back forest (Fig. 3).

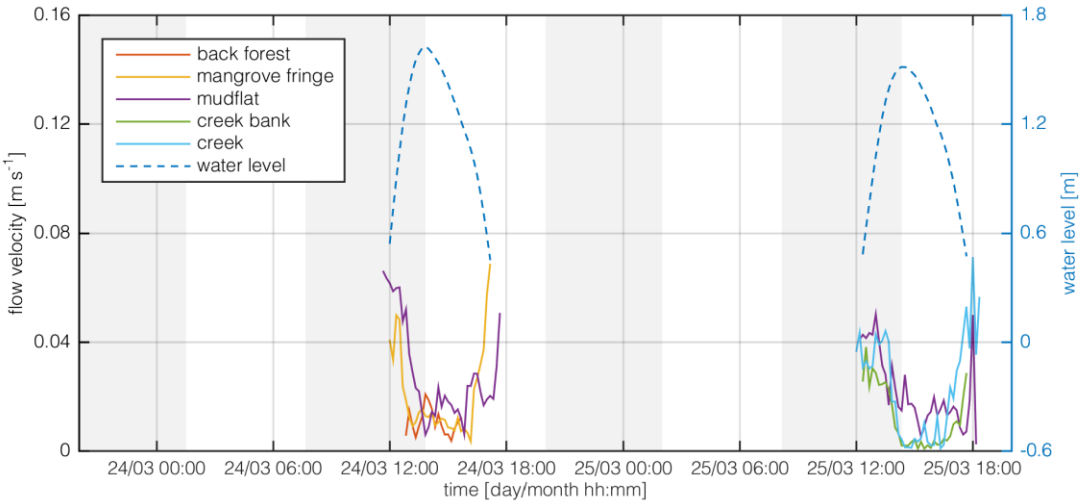

Figure 3.Hydrodynamic results, flow velocities (black) and water levels (blue) of the point observations at the locations: back forest (MA01), mangrove fringe (MA02), mudflat (MAB03), creek bank (MB02).

3.1.3. Sediment dynamics

The observed sediment deposition showed a cross-shore decrease through the mangroves, comparable to the gradient in flow velocities, with the largest deposition observed on the mudflat, i.e. $6.64 \cdot 10^{-2}$ kg m^{-2} and the smallest at the back of the mangrove, i.e. $2.69 \cdot 10^{-3}$ kg m^{-2} (Table 3). The standard deviation of the observed deposition rates was relatively large due to the variance in maximum water levels during the subsequent data collection periods, changing the window for sediment deposition. In addition, we observed some large particles on the sediment traps and possible animal activity as well (by e.g. small snails, mud skippers and crabs).

The grain sizes of the top of the bed (<20 mm below the surface) showed quite some variation (Fig. 4). Observed grain sizes at the mudflat and mangrove fringe (*Sonneratia* patch and creek bank) were quite similar (table 2), with a relatively large amount of clay and silt (Fig. 4; table 2). The sediment fractions at the back of the mangrove and the creek were sandy, the silt/clay fractions were only 10.97 and 7.29 % respectively (table 2). The mean grain size at the back of the mangrove ($3.83 \cdot 10^{2}$ µm) was relatively large, because the large particles, earlier deposited, were never covered by fines, due to the already decreased flow velocities and observed low sediment concentrations. Bed material in the tidal creek was largely sandy (D_{50}: $6.49 \cdot 10^{2}$ µm), due to the concentrated flow and the related high flow velocities. The organic matter content (Table 3) was largest in the center of the mangrove (MA02: mangrove fringe; MB02: creek bank), which was the most vegetated part. The organic matter content of the mangrove locations MA02, MAB03 and MB02 is comparable with other mangrove studies (e.g. Horstman et al. 2015).

Table 2. Observed averaged sediment deposition rates and characteristic sediment properties at each of the monitoring locations in Mandai mangrove: back forest (MA01), mangrove fringe (MA02), mudflat (MAB03), creek bank (MB02) and creek (MB01).

Location	Deposition (standard deviation) [kg m^{-2}]	Mean grain size, D_{50} [µm]	Silt/clay fraction, <63 µm [%]	Organic matter [%]
Back forest	$2.69 \cdot 10^{-3}$ ($1.91 \cdot 10^{-3}$)	$3.83 \cdot 10^{2}$	10.97	2.94
Mangrove fringe	$4.50 \cdot 10^{-2}$ ($1.25 \cdot 10^{-2}$)	$4.40 \cdot 10^{1}$	64.94	15.21
Mudflat	$6.64 \cdot 10^{-2}$ ($4.29 \cdot 10^{-2}$)	$3.89 \cdot 10^{1}$	62.94	10.58
Creek bank	$4.34 \cdot 10^{-2}$ ($1.98 \cdot 10^{-2}$)	$2.73 \cdot 10^{1}$	70.42	15.74
Creek	$4.09 \cdot 10^{-2}$ ($1.95 \cdot 10^{-2}$)	$6.49 \cdot 10^{2}$	7.29	1.50

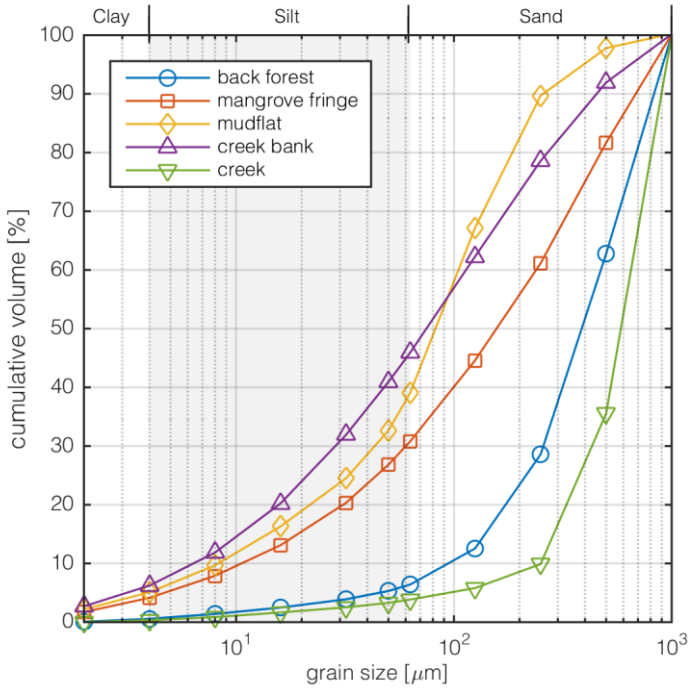

Figure 4. Grain size distribution, defining the relative amount of observed particle sizes at the different measurement locations: back forest (MA01), mangrove fringe (MA02), mudflat (MAB03), creek bank (MB02) and creek (MB01).

3.2. MODEL RESULTS

3.2.1. Calibration

The model was calibrated with the observed flow velocities and sediment deposition rates. Water levels have previously been calibrated and validated rigorously for the SRM. The eddy viscosity and eddy diffusivity of the model had to be adjusted, because of the switching from a 3D to a depth-averaged model. Those parameters should typically be in the range of 1 to 10 $m^2 s^{-1}$ for grid cell dimensions of tens of meters or less and in the range of 10 to 100 $m^2 s^{-1}$ for grid cell dimensions of hundreds of meters or more (Deltares 2015). Both the eddy viscosity and diffusivity have been varied over the range of 1 to 25 $m^2 s^{-1}$ (Table 3) for the model calibration. For the period 24 – 25 march 2015, the computed flow velocities and deposition rates were compared with the observations. Computed deposition rates, only comprising the fine sediments incorporated in the model, have been compared to the fine fractions (<63 µm) of the measured sediment deposition. These deposition rates were obtained by correcting the deposition on the sediment traps for the fraction of fines obtained from the grain size distribution for the same location (table 2). An eddy diffusivity and viscosity of 14 $m^2 s^{-1}$ resulted in the best resemblance of the computed and observed flow velocities during these two days (Fig. 5) and for the computed and observed deposition during the spring high tide at the 24th of March (Fig. 6). The modeled flow velocities showed values comparable to the measured flow velocities, including the asymmetry, due to the sluggish outflow (Furukawa et al. 1996). The simulated deposition of fine sediments showed a highly accurate (spatial) match with the observations (Fig. 6).

Table 3. Model parameters with their related ranges of values that have been developed for the model calibration and sensitivity analysis.

Parameters	[Units]		Model value	Range calibration	Range sensitivity analysis
v	[$m^2\ s^{-1}$]	Eddy viscosity	$1.4 \cdot 10^{1}$	$1.0 \cdot 10^{0}$ - $2.5 \cdot 10^{1}$	-
D	[$m^2\ s^{-1}$]	Eddy diffusivity	$1.4 \cdot 10^{1}$	$1.0 \cdot 10^{0}$ - $2.5 \cdot 10^{1}$	-
w_s	[$mm\ s^{-1}$]	Settling velocity	$1.0 \cdot 10^{-1}$	-	$4.0 \cdot 10^{-2}$ - $2.5 \cdot 10^{-1}$
M	[$kg\ m^{-2}\ s^{-1}$]	Erosion parameter	$1.0 \cdot 10^{-4}$	-	$2.0 \cdot 10^{-5}$ – $5.0 \cdot 10^{-4}$
$\tau_{cr,e}$	[$N\ m^{-2}$]	Critical bed shear stress for erosion	$5.0 \cdot 10^{-1}$	-	$2.5 \cdot 10^{-1}$ - $7.5 \cdot 10^{-1}$
$\tau_{cr,d}$	[$N\ m^{-2}$]	Critical bed shear stress for deposition	$1.0 \cdot 10^{3}$	-	$1.5 \cdot 10^{-1}$ – $1.0 \cdot 10^{3}$

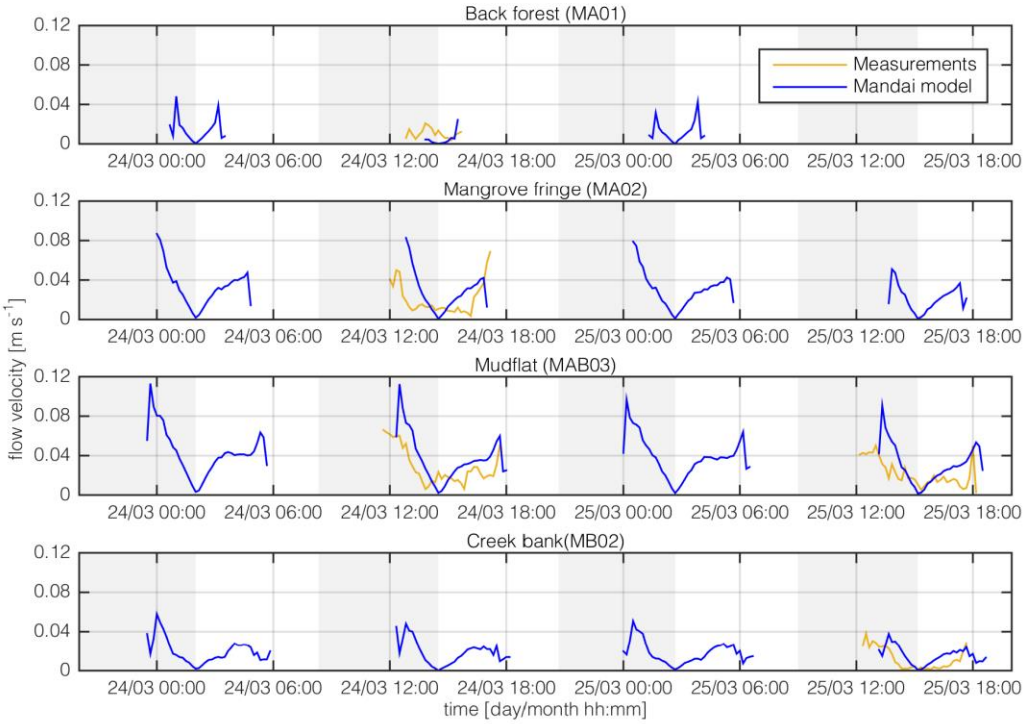

Figure 5. Flow velocities after calibrating the model at the four measurement locations: back forest (MA01), forest fringe (MA02), mudflat (MAB03) and creek bank (MB02). Results are shown for four subsequent tides on 24 and 25 March, for the measurements in the field (yellow) and the output of the model (blue).

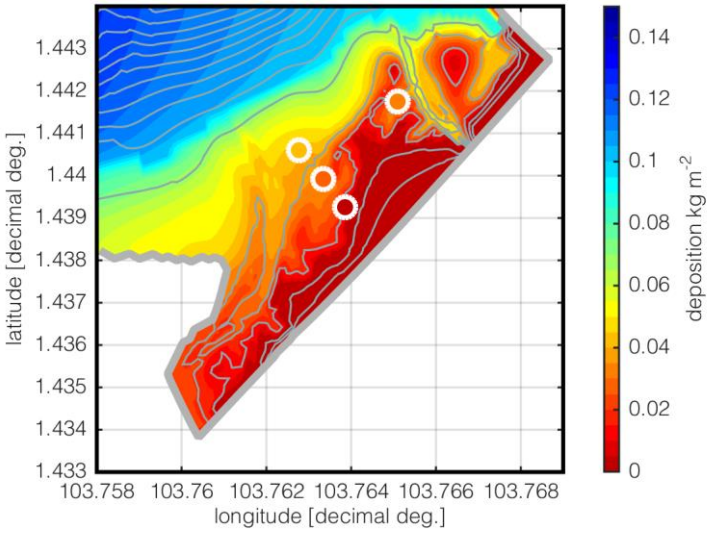

Figure 6. Modeled and measured sediment deposition in Mandai mangrove. The background shows the computed deposition of fine sediments with the model, while the fill color in the white markers shows the measured average (over all measurements) deposition of fines. The depth is shown by the gray contour lines (1 m interval) on top of the modeled deposition.

3.2.2. Sensitivity analysis

To understand the effect of the different parameters on the computed sediment dynamics, and to test the robustness of the model a sensitivity analysis was conducted for various parameters. The parameters analyzed were the settling velocity, the erosion parameter, the critical bed shear stress for erosion and the critical bed shear stress for deposition. The values of these parameters were varied around their initial values according to the ranges in Table 3. These parameters were selected, due to a lack of information regarding their absolute values. The critical bed shear stress for deposition is only analyzed for values lower than the default value, as its initial value was the maximum value for the Delft3D model (Deltares 2015).

Hardly any changes in the computed deposition rates were obtained for variations of the erosion parameter, the critical bed shear stress for erosion and the critical bed shear stress for deposition. This is probably related to the fact that the model is ran with a fixed bed and hence bed dynamics does only comprise the deposition (and re-entrainment) of the supplied suspended sediments. The computed deposition rates were more sensitive to variations in the settling velocity (Fig. 7). The variation in the computed deposition rates compared well with the variation in the deposition rates observed in the field at the creek bank (MB02). The measured deposition at the back of the forest (MA01) was almost zero, whereas the modeled range by the sensitivity analysis was a bit higher. This could be explained by the relatively steep slope at the back of the mangroves and the representation of the monitoring point by a much larger grid cell in the model. In general, a broad range of deposition values could be obtained with the model for a variation of settling velocity values within a plausible range, similar to the observations, which were highly variable as well.

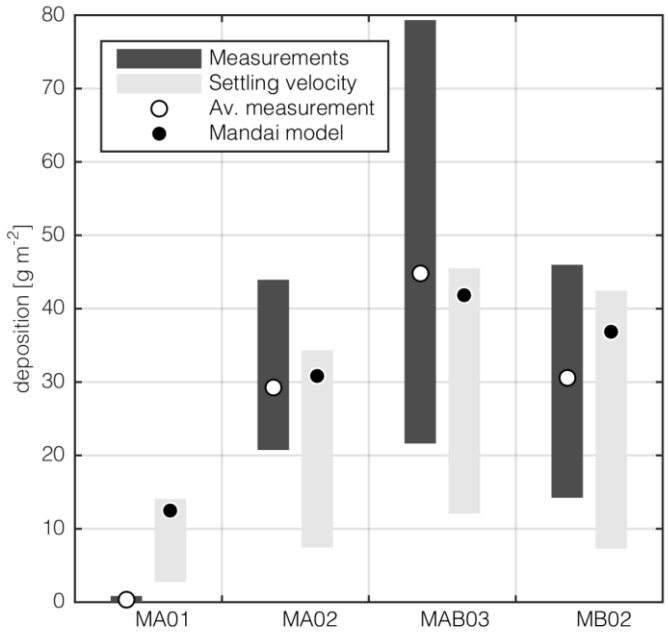

Figure 7. Variation of the observed and computed deposition rates at the four locations: back forest (MA01), forest fringe (MA02), mudflat (MAB03) and creek bank (MB02). The range of measured deposition (for all observations) is shown by the dark gray bars (minimum and maximum respectively at the bottom and top of the bar) with the average deposition indicated by the white marker. The light gray bars show the range of modeled deposition rates computed in the sensitivity analysis, with the black marker showing the deposition for the calibrated model.

3.3. BIOPHYSICAL RESILIENCE OF MANGROVES

The calibrated model was applied to study the biophysical resilience of the Mandai mangrove. Biophysical resilience of mangroves decreases due to human interference resulting in sediment starvation and coastal squeeze. Both processes have been stressing Mandai mangrove, since the construction of the Johor causeway blocked the exchange between the western and eastern side of the Straits of Johor, and since the construction of the Malaysian railway suppressed the landward extension of the mangrove (in combination with SLR), respectively. Both processes were eliminated separately within the calibrated model, to address the potential resilience of such mangroves if these stresses would not exist. Model runs were executed for the time span of 24 – 25 March, resulting in short term-model outcomes. These model outcomes showed the instantaneous reaction and development of the mangroves once the stresses were relieved, which can be used as indicators for the long-term effect of sediment starvation and coastal squeeze.

3.3.1. Sediment starvation

The construction of the Johor causeway (Fig. 1b) in 1913 blocked the tidal exchange between the western and eastern parts of the Straits of Johor (Friess et al. 2012). For this scenario, the closure of the Straits was assumed to be a major cause of the reduced sediment supply to Mandai mangrove. Hence, the model set-up has been adapted for analyzing the influence of sediment starvation: the Johor causeway was modified from a closed boundary to an open boundary, with astronomical forcing by water levels similar to boundary conditions imposed on the western open boundary (see section 3.2.2.). This new open boundary is closely located to the study site of Van Maren et al. (2014) where SSCs have been observed to be about 15 mg l^{-1} ($1.5 \cdot 10^{-2}$ kg m^{-3}). This value is imposed as a constant boundary condition for the SSC at the new open boundary at the location of the causeway. The model was executed for a series of adjacent SLR scenarios (0.0:0.1:0.5m),

while maintaining the existing tidal amplitudes. In addition, the vegetation density was varied (0% - 200%), along with SLR.

The computed hydrodynamics for initial runs with tidal exchange between the eastern and western end of the Straits of Johor without any SLR during 24 and 25 March only showed minor deviations with respect to the original results. The opening of the causeway resulted in general in increasing flow velocities (differences smaller than 0.01 m s^{-1}) during ebb tides. Computed deposition rates increased consistently throughout the study site (Fig. 8.a), following the topography.

Simulated deposition rates were analyzed by aggregating the deposition per grid cell into three different zones (Fig. 9.a): the mangrove fringe (I), the central mangrove (II), the back of the mangrove (III), all subdivided by characteristic heights derived from the topography of the model. The deposition of fine sediments was more than 100% larger than model outcomes with SLR from the initial model (Fig. 10.a). Zone I showed an increase of almost 300%. The sediment deposition showed a larger increase along with increasing SLR than the increase in deposition from the initial model without tidal exchange, i.e. a steeper gradient for the deposition could be observed for model runs with two open boundaries (Fig. 9.a).

According to these results sediment starvation has major influences on mangroves. Enabling tidal exchange, i.e. a 200% sediment influx compared to outcomes from the original model, results in deposition rates of almost 300%. The resilience of the mangrove increases due to steeper deposition gradients along to increasing rates of SLR.

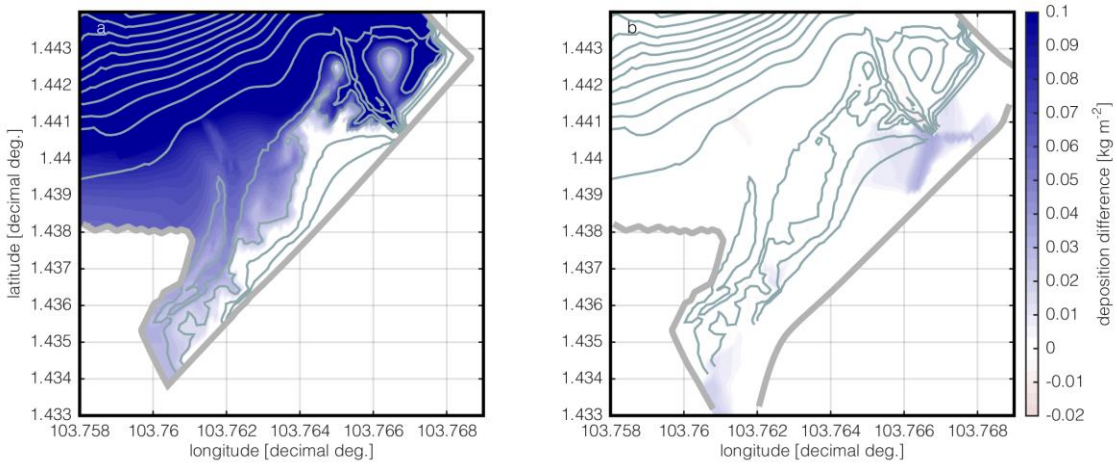

Figure 8. Differential maps for the computed sedimentation compared to values computed with the original model for: (a) a scenario with free exchange between the eastern and western part of the Straits of Johor and (b) a scenario with an open basin added at the back of Mandai mangrove.

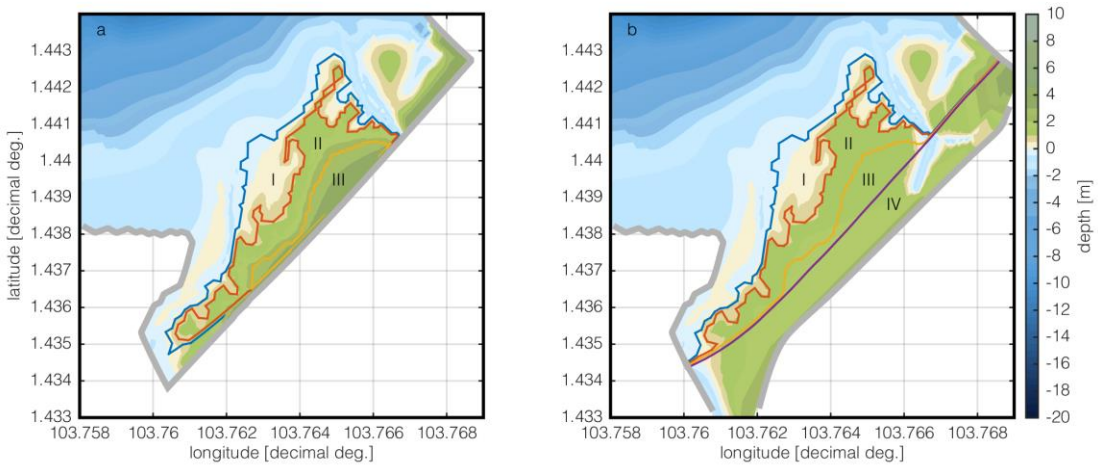

Figure 9. Bathymetry of (a) the original model and (b) the extended model for the scenario regarding coastal squeeze. The contours indicate the boundaries of the characteristic zones: the area between the blue and red line, zone I, shows the fringe, the area between the red and yellow line, zone II, shows the central mangrove, the area between the yellow line and southeastern border and the yellow or purple line (in b), zone III, shows the back of the forest and the area between the purple line and the southeastern border (b), area IV, shows the developed basin.

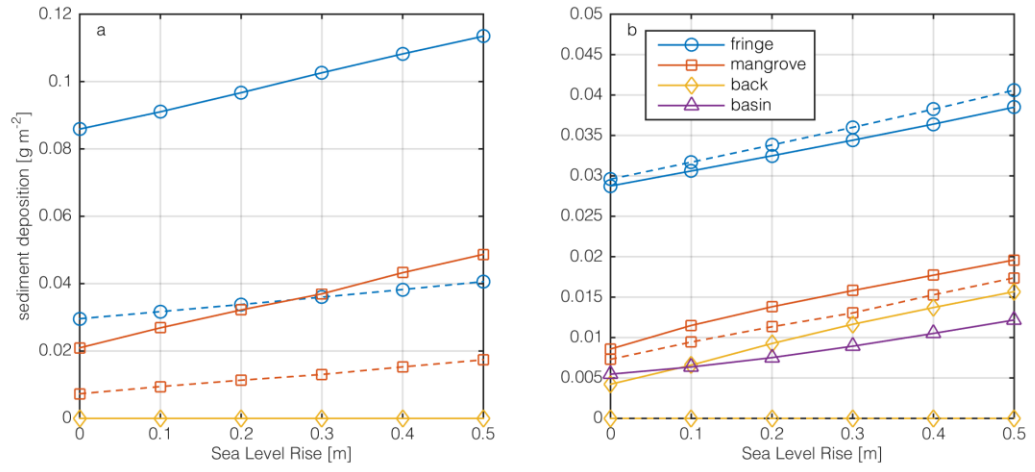

Figure 10. Deposition of fine sediments within the characteristic zones of the mangrove for the original model (dashed lines) and for the scenario's with (continuous lines). The sediment deposition in g m^{-2} is showed for the scenarios with an open boundary imposed at the Johor Causeway (a) and for the scenario with an open basin at the back of the mangrove (b).

3.3.2. Coastal squeeze

Landward development of Mandai mangrove is currently suppressed, causing a decreased resilience, especially in combination with SLR. Model runs were executed to study the effect of this coastal squeeze. The model was executed for a similar series of adjacent SLR values as the sediment starvation scenario (see section 3.3.1.), combined with varying vegetation densities as well. The results were compared to an adapted model in which the topography was changed as to include an open basin landward of the mangroves (at the location where currently the Singapore-Malaysia railway is and some grassland is; Fig. 1.f). Simultaneously the bed level at the back of the mangrove was decreased from a maximum of +4.0 m MSL to +1.5m MSL, as to facilitate tidal exchange. The elevation in the basin increased to +3.0m and +4.0m MSL at the eastern and western end of the basin, respectively. The tidal creeks were extended into the basin as well, cutting through the new topography. The Manning roughness coefficient for the new basin was based on values for pasture and bare soil (just excavated) and the value was set to: 0.05 s $m^{-1/3}$ (Chow 1959).

Only minor differences in deposition were observed for initial runs with the landward basin without any SLR. These minor differences were the slowly filling up creek extensions (Fig. 8.b). However, model outcomes show an increasing tidal prism with increasing SLR. Flow velocities show major differences at the back forest (MA01) and within the mangrove fringe (MA02), which can be explained by the longer and lower mangrove stretch not decelerating the flow as much as before and the increased throughput of water towards the back of the mangrove. Computed flow velocities and deposition rates influenced by different vegetation densities hardly showed any changes.

Simulated deposition rates were analyzed by aggregating the deposition per grid cell in similar zones as the previous scenario (see section 3.3.1.). In addition the imposed basin (zone IV) was added to the three zones (Fig. 9.b). The deposition of fine sediments computed for this scenario showed major differences with the original model (Fig. 9b). Deposition at zone I showed a small decrease, due to the higher flow velocities, transporting more suspended sediments into the mangrove. Deposition in zone II increased with approximately 12% and deposition in zone III increased, as well as in zone IV. The computed deposition in all zones increased structurally (approximately linear) as a result of increasing SLR (Fig. 10.b).

According to these results, an increasing mangrove extent results in an increasing resilience, due to the higher flow velocities and increased throughput of water facilitating greater sediment inputs. These increasing sediment inputs result in more sediment deposition over the whole mangrove extent. The deposition increases further with SLR coinciding, giving the mangrove better possibilities to maintain its position in the tidal frame.

4. DISCUSSION

Wetlands show resilient behavior to environmental changes like SLR by means of their biophysical feedback mechanisms (e.g. Cahoon et al. 2006). However, these natural feedback mechanisms can be compromised by anthropogenic stresses (see Kirwan et al. 2013), affecting the natural resilience. The results of the scenario analysis showed that anthropogenic influenced mangroves indicated an increasing resilience to the absence of coastal squeeze and sediment starvation. In addition the results indicated that vegetation can degredade to an extent that it does not contribute to the mangroves resilience anymore, while studies into less influenced mangroves showed a resilient capacity of the vegetation (e.g. Horstman et al. 2015).

4.1. ANTHROPOGENICALLY STRESSED MANGROVES

Typical features of anthropogenic influenced mangroves are e.g. sediment starvation, fragmented vegetation patches and non-dynamical back boundaries (e.g. Strong et al. 1994; Kirwan et al. 2013). Mandai mangrove is stressed by all these phenomena. Part of the measured and tagged vegetation in 2011-2012 (Leong), was already degraded towards the field campaign of spring 2015, indicating ongoing fragmentation of the mangroves. Point data were collected to indicate the typical hydrodynamics and sediment dynamics during different periods of tidal flooding. The resulting flow velocities (creek flow and sheet flow) emphasized the impact of a non-natural development: flow velocities were significantly smaller than in studies of natural

mangroves (e.g. Van Santen et al. 2007; Horstman et al. 2013; Horstman et al. 2015). Flow velocities were low due to the Johor causeway, blocking any longshore flows, and due to the very limited inland extent of the mangrove, limiting the tidal prism (i.e. the amount of water moving in and out of the forest every tide).

Model runs explicitly accounting for the mangrove vegetation, including the recently appeared *Sonneratia* saplings, were executed with varying vegetation densities, ranging between 0% - 200%. The results showed hardly any changes in the hydrodynamics and sediment dynamics. This is a strong indication of a non-resilient mangrove system, where biophysical feedback mechanisms are reduced due to anthropogenic pressure. A positive feedback between instantaneous vegetation density change and deposition has been proven before by different studies in wetlands and flumes which are not influenced by (or only influenced by unavoidable) anthropogenic effects (e.g. Gleason et al. 1979; Bouma et al. 2007; Horstman et al. 2015). This biophysical feedback between vegetation and accretion, described by e.g. Kirwan et al. (2013), is not present in these mangroves that are severely stressed by anthropogenic influences.

4.2. INITIAL RESPONSE VERSUS LONG TERM IMPLICATIONS

The developed numerical model only showed outcomes of short -term simulations. These results were used to explore the mangroves' adaptability and development under instantaneous adaptations of the environment. This model set-up was changed to mimic conditions without some of the human induced stresses to explore the adaptive capacity of the mangrove (to future changes) if some of these stresses were (to be) relieved

4.2.1. Hindcasts

The sensitivity of the mangroves' resilience to sediment starvation was simulated by allowing water and sediment exchange across the currently closed Johor causeway (Fig. 1.b). During low tide, this now open boundary allows an outflow of suspended sediments as well. The computed instantaneous response of the mangrove showed a convincing increase of deposition. Deposition throughout Mandai increased if the tidal exchange between the eastern and western side of the Straits of Johor was open.

These results indicate that, if the causeway would not have been blocking the sediment dynamics in the Straits of Johor, the higher SSC concentrations would have facilitated greater deposition rates. This would probably have resulted in an increased mangrove extent nowadays, with an increased adaptive capacity due to the greater sediment availability. This is a clear indicator for the impacts of sediment starvation on the development of coastal wetlands , which is a serious concern given the 26% worldwide decrease of sediment influxes in coastal zones (Syvitski et al. 2005).

The impact of SLR in Mandai mangrove has not been quantified in the past (Friess et al. 2012). Observations showed that *Sonneratia* saplings were established and developing on the mudflat, indicating the absence of 'ecological drowning' due to SLR. However, vegetation was degrading in the center of the mangrove. Clear evidence for coastal squeeze could hence not be found yet, despite of the suppressed landward development.

Biophysical feedbacks allow coastal wetlands to survive conditions under which they cannot develop (D'Alpaos et al. 2012; Kirwan et al. 2013). Model runs with varying vegetation densities (0% - 200%), in combination with the scenarios for sediment starvation and coastal squeeze, indicated that the biophysical feedbacks were no longer contributing to the development of the mangrove. Hydrodynamics and sediment dynamics showed hardly any changes when comparing simulation results of these scenarios with different vegetation densities to the runs with a vegetation density of 100%. This lacking response to changes in the vegetation is an indicator of a decreased resilience. This could be caused by sediment starvation, and has been observed before (e.g. Blum et al. 2009). Model outcomes showed that sediment starvation caused decreasing deposition rates. A decreased deposition rate or even erosion exposes root systems of the mangroves' vegetation to physical disturbance, potentially resulting in degrading vegetation. Balke et al. (2013) showed this for the establishment of mangrove seedlings. In the absence of sediment starvation, the biophysical feedbacks would have been intact, preventing degrading vegetation and fragmentation, resulting in no blank spots exposed to erosion.

4.2.2. Forecasts

Observations of the present development of Mandai were quite contradictory: mature trees at the forest fringe were degrading, while *Sonneratia* patches recently settled at the mudflat. Fragmented vegetation results in a loss of stabilizing feedback mechanisms (Morris et al. 2002; Kirwan et al. 2010; Kirwan et al. 2013) and this was observed for instance around the tidal creek in Mandai. Given the relatively low sediment deposition rates observed in Mandai (also compared to other studies, e.g. Horstman et al. (2015)), especially taking into account that the data were collected during near-spring tides, the current degradation of Mandai mangrove is likely to continue in the (near) future. This study shows that this negative trend could be reversed if the sediment supply would be restored or if the tidal dynamics within the mangroves were increased.

Coastal squeeze is a serious threat for mangroves, and coastal wetlands in general, due to the predicted increasing sea levels (Kirwan et al. 2013). Mandai mangrove is constrained by the hard landward boundary at present, reducing the tidal exchange and limiting the sediment deposition throughout the mangroves. When SLR takes place, the recently settled vegetation at the mudflat is likely to drown, potentially followed by ecological drowning of the entire mangrove. Creating a basin at the back of the mangrove is shown to result in enhanced deposition throughout the mangrove, increasing its chances to keep up with SLR and meanwhile allowing the mangroves to extend landward (to higher grounds) as well. The model outcomes indicated that mangroves are more resilient when landward development is possible, resulting in natural development along SLR.

The developed model only showed short term calculations for conditions during which deposition is dominant. Wave action, causing erosion in wetland, is very limited in Mandai due to its sheltered location in the Straits of Johor and hence was neglected. Extreme weather events are also causing erosion in wetlands (Bell et al. 2013; Roebeling et al. 2013; Krauss et al. 2014). Erosion caused by extreme weather events is not taken into account in this study because it does not show the prevailing conditions nor the restoring positive biophysical feedback mechanisms.

5. CONCLUSIONS

This combined field and model study showed the impacts of human interference on the biophysical interactions in mangroves. Observations in a disturbed mangrove stressed by sediment starvation and coastal squeeze showed low flow velocities and low sediment deposition rates in combination with a fragmented and scattered vegetation pattern. The numerical model of the hydrodynamics and sediment dynamics in this area showed reasonable approximations of the flow velocities and sediment deposition rates observed in the field. Simulations with this model provided insight in the instantaneous response of the mangrove when sediment starvation and coastal squeeze were reduced. The model results showed increased deposition rates within the mangrove when sediment supplies were restored. In addition, a faster increase of sediment deposition rates can be observed when restored sediment supplies were combined with increasing SLR. A reduction of the coastal squeeze by extending the intertidal area in the inland directions resulted in increasing flow velocities and deposition rates as well. A comparison between these scenario runs and the current state of the mangrove showed a decrease in biophysical interaction and even a total loss of the contribution of vegetation to the stability of the current state mangrove. The human interference, contributing to sediment starvation and coastal squeeze, has evidently decreased the mangrove's resilience. Future sea-level rise might further compromise this resilience. More importantly, relieving these human induced stresses, found to enhance sediment deposition rates, facilitates an increased resilience to future changes such as sea-level rise.

ACKNOWLEDGEMENTS

The research presented in this work was financially supported by the Dutch KNAW Fonds Ecologie 2015 (UPS/375/Eco/J1514). Presented field work has been executed under the research permit of NParks Singapore (NP/RP936). We greatly acknowledge P. Taillardat, D. Richards, C. Lyons and others for their assistance during the field campaign. W. K. Lee is gratefully acknowledged as well for his help during the data collection and delivering vegetation data. Thank you to S. Tay and S. K. Ooi for delivering the model, and thank you to E. Segovia Estrada and L. Prabhai for the lab assistance. L. van IJzerloo is acknowledged for the sediment analysis. NWO-STW is acknowledged for giving B. W. Borsje the possibility to be part of this study and The Royal Society of New Zeeland's Marsden Fund for giving E. M. Horstman the possibility to be part of this study.

REFERENCES

Balke, T., E. L. Webb, E. van den Elzen, D. Galli, P. M. J. Herman and T. J. Bouma (2013). Seedling establishment in a dynamic sedimentary environment: a conceptual framework using mangroves. Journal of Applied Ecology 50: 740-747.

Bell, J. and C. E. Lovelock (2013). Insuring mangrove forests for their role in mitigating coastal erosion and storm -surge: an Australian case study. Wetlands 33: 279-289.

Blum, M. D. and H. H. Roberts (2009). Drowning of the Mississippi Delta due to insufficient sediment supply and global sea-level rise. Nature Geoscience 2: 488-491.

Bouma, T. J., L. A. van Duren, S. Temmerman, T. Claverie, A. Blanco-Garcia, T. Ysebaert and P. M. J. Herman (2007). Spatial flow and sedimentation patterns within patches of epibenthic structures: Combining field, flume and modelling experiments. Continental Shelf Research 27: 1020-1045.

Cahoon, D. R., P. F. Hensel, T. Spencer, D. J. Reed, K. L. McKee and N. Saintilan (2006). Coastal wetland vulnerability to relative sea-level rise: wetland elevation trends and process controls. Wetlands and Natural Resource Management. J. A. Verhoeven, B. Beltman, R. Bobbink and D. Whigham, Springer Berlin Heidelberg. 190: 271-292.

Chanson, H., M. Trevethan and S. Aoki (2008). Acoustic Doppler Velocimetry (ADV) in small estuary: field experience and signal post-processing. Flow Measurement and Instrumentation 19: 307-313.

Chow, V. (1959). Open channel hydraulics. New York, McGraw-Hill.

D'Alpaos, A., C. Da Lio and M. Marani (2012). Biogeomorphology of tidal landforms: physical and biological processes shaping the tidal landscape. Ecohydrology 5: 550-562.

De Groot, R., L. Brander, S. van der Ploeg, R. Costanza, F. Bernard, L. Braat, M. Christie, N. Crossman, A. Ghermandi, L. Hein, S. Hussain, P. Kumar, A. McVittie, R. Portela, L. C. Rodriguez, P. ten Brink and P. van Beukering (2012). Global estimates of the value of ecosystems and their services in monetary units. Ecosystem Services 1: 50-61.

Deltares (2015). User manual DELFT3D-FLOW. Deltares. Delft.

Doody, J. P. (2004). 'Coastal squeeze'— an historical perspective. Journal of Coastal Conservation 10: 129-138.

Duarte, C. M., W. C. Dennison, R. J. W. Orth and T. J. B. Carruthers (2008). The Charisma of Coastal Ecosystems: Addressing the Imbalance. Estuaries and Coasts 31: 233-238.

Friess, D. A., K. W. Krauss, E. M. Horstman, T. Balke, T. J. Bouma, D. Galli and E. L. Webb (2012). Are all intertidal wetlands naturally created equal? Bottlenecks, thresholds and knowledge gaps to mangrove and saltmarsh ecosystems. Biological reviews 87: 346-366.

Friess, D. A., J. Phelps, R. C. Leong, W. K. Lee, A. K. S. Wee, N. Sivasothi, R. R. Y. Oh and E. L. Webb (2012). Mandai mangrove, Singapore: Lessons for the conservation of Southeast Asia's mangroves. The Raffles Bulletin of Zoology: 55-65.

Furukawa, K. and E. Wolanski (1996). Sedimentation in mangrove forests. Mangroves and Salt Marshes 1: 3-10.

Gleason, M. L., D. A. Elmer, N. C. Pien and J. S. Fisher (1979). Effects of stem density upon sediment retention by salt marsh cord grass, Spartina alterniflora loisel. Estuaries 2: 271-273.

Hasan, G. M. J., D. S. van Maren and H. F. Cheong (2012). Improving hydrodynamic modeling of an estuary in a mixed tidal regime by grid refining and aligning. Ocean Dynamics 62: 395-409.

Horstman, E. M., C. M. Dohmen-Janssen, T. J. Bouma and S. J. M. H. Hulscher (2015). Tidal-scale flow routing and sedimentation in mangrove forests: Combining field data and numerical modelling. Geomorphology 228: 244-262.

Horstman, E. M., C. M. Dohmen-Janssen, T. J. Bouma and S. J. M. H. Hulscher (2015). Tidal-scale flow routing and sedimentation in mangrove forests: Combining field data and numerical modelling. Geomorphology 228: 244-262.

Horstman, E. M., C. M. Dohmen-Janssen and S. J. M. H. Hulscher (2013). Flow routing in mangrove forests: A field study in Trang province, Thailand. Continental Shelf Research 71: 52-67.

Horstman, E. M., C. M. Dohmen-Janssen and S. J. M. H. Hulscher (2013). Flow routing in mangrove forests: a field study in Trang province, Thailand. Continental Shelf Research 71: 52-67.

Hu, K., P. Ding, Z. Wang and S. Yang (2009). A 2D/3D hydrodynamic and sediment transport model for the Yangtze Estuary, China. Journal of Marine Systems 77: 114-136.

Jones, C. G., J. H. Lawton and M. Shachak (1994). Organisms as ecosystem engineers. Oikos 69: 373-386.

Jones, C. G., J. H. Lawton and M. Shachak (1997). Positive and negative effects of organisms as physical ecosystem engineers. Ecology 78: 1946-1957.

Kernkamp, H. W. J., H. A. H. Petit, H. Gerritsen and E. D. de Goede (2005). A unified formulation for the three-dimensional shallow water equations using orthogonal co-ordinates: theory and application. Ocean Dynamics 55: 351-369.

Kirwan, M. L., G. R. Guntenspergen, A. D'Alpaos, J. T. Morris, S. M. Mudd and S. Temmerman (2010). Limits on the adaptability of coastal marshes to rising sea level. Geophysical Research Letters 37.

Kirwan, M. L. and P. Megonigal (2013). Tidal wetland stability in the face of human impacts and sea-level rise. Nature 504: 53-60.

Krauss, K. W., J. A. Allen and D. R. Cahoon (2003). Differential rates of vertical accretion and elevation change among aerial root types in Micronesian mangrove forests. Estuarine, Coastal and Shelf Science 56: 251-259.

Krauss, K. W., D. R. Cahoon, J. A. Allen, K. C. Ewel, J. C. Lynch and N. Cormier (2010). Surface elevation change and susceptibility of different mangrove zones to sea-level rise on pacific high islands of micronesia. Ecosystems 13: 129-143.

Krauss, K. W., K. L. McKee, C. E. Lovelock, D. R. Cahoon, N. Saintilan, R. Reef and L. Chen (2014). How mangrove forests adjust to rising sea level. New Phytologist 202: 19-34.

Kurniawan, A., S. K. Ooi, S. Hummel and H. Gerritsen (2011). Sensitivity analysis of the tidal representation in Singapore Regional Waters in a data assimilation environment. Ocean Dynamics 61: 1121-1136.

Lee, W. K. (2015). In progress.

Leong, R. C. Unpublished data.

Lesser, G. R., J. A. Roelvink, J. A. T. M. van Kester and G. S. Stelling (2004). Development and validation of a three-dimensional morphological model. Coastal Engineering 51: 883-915.

Mazda, Y., E. Wolanski and P. V. Ridd (2007). The role of physical processes in mangrove environments: manual for the preservation and utilization of mangrove ecosystems, Terrapub.

Mckee, K. L., R. C. Cahoon and I. C. Feller (2007). Caribbean mangroves adjust to rising sea level through biotic controls on change in soil elevation. Global Ecology and Biogeography 16: 545-556.

Morris, J. T., P. V. Sundareshwar, C. T. Nietch, B. Kjerfve and D. R. Cahoon (2002). Responses of coastal wetlands to rising sea level. Ecology 83: 2869-2877.

Pawlowicz, R., B. Beardsley and S. Lentz (2002). Classical tidal harmonic analysis including error estimates in Matlab using T_TIDE. Computers and Geosciences 28: 929-937.

Roebeling, P. C., L. Costa, L. Magalhães-Filho and V. Tekken (2013). Ecosystem service value losses from coastal erosion in Europe: historical trends and future projections. Journal of Coastal Conservation 17: 389-395.

SonTek (1997). Pulse Coherent Doppler Processing and the ADV Correlation Coefficient. San Diego, SonTek.

Strong, A. M. and B. G. Thomas (1994). Patterns of deforestation and fragmentation of mangrove and deciduous seasonal forests in the Upper Florida Keys. Bulletin of Marine Science 54: 795-804.

Syvitski, J. P. M., C. J. Vörösmarty, A. J. Kettner and P. Green (2005). Impact of humans on the flux of terrestrial sediment to the global coastal ocean. science 308: 376-380.

Temmerman, S., T. J. Bouma, G. Govers, Z. B. Wang, M. B. De Vries and P. M. J. Herman (2005). Impact of vegetation on flow routing and sedimentation patterns: Three-dimensional modeling for a tidal marsh. Journal of Geophysical Research: Earth Surface 110: F04019.

Thampanya, U., J. E. Vermaat, S. Sinsakul and N. Panapitukkul (2006). Coastal erosion and mangrove progradation of Southern Thailand. Estuarine, Coastal and Shelf Science 68: 75-85.

Valiela, I., J. L. Bowen and J. K. York (2001). Mangrove Forests: One of the World's Threatened Major Tropical Environments. BioScience 51: 807-815.

Van Maren, D. S., S. C. Liew and G. M. J. Hasan (2014). The role of terrestrial sediment on turbidity near Singapore's coral reefs. Continental Shelf Research 76: 75-88.

Van Maren, D. S. and J. C. Winterwerp (2012). The role of flow assymetry and mud properties on tidal flat sedimentation. Continental Shelf Research 60: S71-S84.

Van Santen, P., P. G. E. F. Augustinus, B. M. Janssen-Stelder, S. Quartel and N. H. Tri (2007). Sedimentation in an estuarine mangrove system. Journal of Asian Earth Sciences 29: 566-575.

Victor, S., Y. Golbuu, E. Wolanski and R. H. Richmond (2004). Fine sediment trapping in two mangrove-fringed estuaries exposed to contrasting land-use intensity, Palau, Micronesia. Wetlands Ecology and Management 12: 277-283.

Webb, E. L., D. A. Friess, K. W. Krauss, D. R. Cahoon, G. R. Guntenspergen and J. Phelps (2013). A global standard for monitoring coastal wetland vulnerability to accelerated sea-level rise. Nature Climate Change 3: 458-465.

Webb, E. L., N. R. A. Jachowski, J. Phelps, D. A. Friess, M. M. Than and A. D. Ziegler (2014). Deforestation in the Ayeyarwady Delta and the conservation implications of an internationally-engaged Myanmar. Global Environmental Change 24: 321-333.

Whitehouse, R. J. S., R. Soulsby, W. Roberts and H. Mitchener (2000). Dynamics of estuarine muds, Thomas Telfort Ltd. and HR Wallingford.

Winterwerp, J. C. (2002). On the flocculation and settling velocity of estuarine mud. Continental Shelf Research 22: 1339-1360.

Wolanski, E., R. J. Gibbs, Y. Mazda, A. Mehta and B. King (1992). The role of turbulence in the settling of mud flocs. Journal of coastal Research 8: 35-46.

Yee, A. T. K., W. F. Ang, S. Teo, S. C. Liew and H. T. W. Tan (2010). The present extent of mangrove forests in Singapore. Nature in Singapore 3: 139-145.